Korean J. Chem. Eng., 33(12), 3359-3366 (2016)
DOI: 10.1007/s11814-016-0203-6

pISSN: 0256-1115
eISSN: 1975-7220

The effect of promoters on the CO_2 reforming activity and coke formation of nanocrystalline Ni/Al_2O_3 catalysts prepared by microemulsion method

Mohammad Hossein Aboonasr Shiraz*,, Mehran Rezaei*,**,†, and Fereshteh Meshkani***

*Catalyst and Advanced Materials Research Laboratory, Chemical Engineering Department, Faculty of Engineering, University of Kashan, Kashan, Iran
**Institute of Nanoscience and Nanotechnology, University of Kashan, Kashan, Iran
(*Received 24 February 2016 • accepted 12 July 2016*)

Abstract−Mesoporous nanocrystalline nickel-alumina promoted catalysts with high surface area were prepared by microemulsion (ME) method and employed in dry reforming of methane reaction. The catalysts were characterized by X-ray diffraction (XRD), Brunauer-Emmett-Teller surface area analysis (BET), temperature programmed reduction (TPR) and temperature programmed oxidation (TPO) techniques. The results showed that the prepared catalysts had high porosity with great surface area and small crystallite size. Among the K_2O, MgO, CaO and BaO promoters, the MgO promoter showed considerable effect on catalytic performance and coke suppression of catalyst.

Keywords: Microemulsion, Nanocrystalline, Nickel Catalyst, Dry Reforming, Promoter

INTRODUCTION

Recently, the most research interests are in the area of light hydrocarbons reforming, because it uses greenhouse gases such as carbon dioxide and methane. These two gases can be converted to the two useful gasses (H_2 and CO); simply called syngas. Dry reforming (DRM) is a useful method which alters the carbon dioxide and methane into beneficial gases ($CO_2+CH_4\leftrightarrow 2CO+2H_2$). Dry reforming for production of syngas has several advantages both economically and also environmentally. This process relies on some positive aspects: first, it regulates H_2/CO ratio in terms of 1 : 1, and second it decreases the two gases' participation in global warming and finally better use in chemical energy transmission [1-3].

From the view of an industrial process, Ni-based catalysts are mostly used due to their low cost; but the major challenge is coke deposition over the nickel catalyst surface and the fast deactivation during CO_2 reforming reaction [4-7]. The coke comes from two main reactions [8-10]:

$$CH_4\leftrightarrow C+2H_2 \quad \Delta H^0_{298}=75\ \text{kJ/mol (Methane decomposition)} \qquad (1)$$

$$2CO\leftrightarrow C+CO_2 \quad \Delta H^0_{298}=-172\ \text{kJ/mol (Boudouard reaction)} \qquad (2)$$

To overcome this problem, some alkaline and alkaline earth promoters have been used to limit the carbon formation on Ni catalysts [11,12]. The addition of basic promoters (alkali and alkaline earths metal oxides) increases the adsorption of CO_2 on the catalyst surface [13-15]. By increasing the basicity of the catalyst, the reaction of CO_2 with the deposited carbon increased and led to improving the catalytic stability. MgO enhances the catalytic properties of Ni/Al_2O_3 catalyst in dry reforming of methane [16]. Shen et al. reported that the $Ni/MgAl_2O_4$ catalyst showed high resistance against sintering and carbon formation in dry reforming of methane [17]. The high resistance of this catalyst against carbon formation was related to the formation of MgO-NiO solid-solution. In this condition, the basic surface with small nickel particles on the surface of the solid solution makes an excellent situation for the prevention of coke deposition [18,19].

Monodisperse colloidal metal particles were prepared by Boutonnet et al. in the early 1980s [20]. With strong nickel support interaction in the catalyst, nickel sintering and carbon deposition can be avoided [21]. Microemulsion can prepare a good interaction between active metal and catalyst support. Reverse microemulsion can prepare an adequate environment for reactants to chemically produce nanosized particles and control their disposition and composition [20].

We prepared Ni/Al_2O_3 catalyst with microemulsion method for dry reforming reaction. The effect of K_2O, MgO, CaO, and BaO as promoters and the effect of different MgO contents were investigated on the catalytic performance of the $7.5Ni/Al_2O_3$ catalyst.

EXPERIMENTAL

1. Catalysts Preparation

Ni/Al_2O_3 catalyst with 7.5 wt% nickel was made by microemulsion method according to our previously published paper [22]. Triton X-100 and 1-butanol were mixed together. The concentration of Triton X-100 in 1-butanol was chosen as 0.55 g/ml. After that, a suitable concentration of $Ni(NO_3)_2{\cdot}6H_2O$ aqueous solution was added to the prepared mixture. The mixture was stirred for 30 min. and then the triethylamine was added dropwise to the prepared mixture. The nanoparticles of $Ni(OH)_2$ were formed in the microemulsion (w/o) by addition of 15 ml triethylamine. In the next step, aluminum triisopropoxide was added to the prepared

†To whom correspondence should be addressed.
E-mail: rezaei@kashanu.ac.ir

microemulsion containing the $Ni(OH)_2$ particles and the hydrolysis of aluminum triisopropoxide was done for 30 min under vigorous stirring. After that the suspension was filtered and washed with distilled water and ethanol to remove any residual surfactant. Then the washed suspension was dried at 85 °C and calcined at 500 °C for 3 h.

Promoters were added to the prepared nickel catalyst by a wet impregnation method. For this purpose, the dehydrated catalyst was impregnated with aqueous solutions of promoter (X) precursors {KNO_2 (96% purity, Loba Chemie), $Mg(NO_3)_2{\cdot}6H_2O$ (98% purity, Loba Chemie), $Ca(NO_3)_2{\cdot}4H_2O$ (99% purity, Loba Chemie), and $Ba(NO_3)_2$ (99% purity, Merck)} under stirring for 4 h at room temperature. The promoted catalysts were dried at 80 °C for 10 h and calcined at 500 °C for 3 h with a heating rate of 3 °C/min.

2. Characterization

The structural properties of the samples were investigated by X-ray diffraction (XRD) analysis using an X-ray diffractometer (PAN analytical X'Pert-Pro). The surface areas of the prepared catalysts were determined by nitrogen adsorption at −196 °C using a Tristar 3020 analyzer (Micromeritics). Prior to analysis the prepared samples were degassed under an inert atmosphere (N_2) for 2 h at 250 °C. The pore size distribution of the samples was calculated from the desorption branch of the N_2 adsorption/desorption isotherm by the Barrett, Joyner and Halenda (BJH) method. The reduction behavior of the calcined catalysts was evaluated by temperature programmed reduction (TPR) using a Micromeritics chemisorb 2750 instrument. For this purpose, the calcined catalyst (100 mg) was heated (10 °C/min) in a reducing gaseous mixture (20 ml/min, H_2 : Ar=10 : 90). Before the analysis, the catalysts were degassed under an Ar atmosphere at 250 °C for 1 h. The amount of H_2 uptake during the reduction process was determined by a thermal conductivity detector (TCD). The carbon deposited over the spent catalysts was evaluated using temperature-programmed oxidation (TPO) analysis with a similar apparatus as mentioned for TPR analysis. In this analysis a gas stream (20 mL/min) of a O_2 : He (5 : 95) mixture was passed over 50 mg of the spent catalyst and the temperature increased with a desired heating rate (10 °C/min). Surface morphology of the prepared catalysts was studied by a scanning electron microscope (SEM, Vega@Tescan).

3. Catalytic Evaluation

The catalytic activity and stability of the prepared samples were evaluated in a vertical quartz fixed-bed reactor (inner diameter=7 mm) under atmospheric pressure. Prior to the reaction, different calcined catalysts were reduced in a pure flow of H_2 gas (30 mL/min) at 700 °C for 3 h and cooled to 550 °C. The reactant gas feed (CH_4 and CO_2) with different ratios was passed over the catalyst bed and the catalytic performance tests were performed at different reaction temperatures (550-700 °C). The volume percent of reactants and products were determined using a gas chromatograph (Shimadzu 16A) equipped with a TCD and a Carboxen 1000 column.

RESULTS AND DISCUSSION

1. Physical Properties of the Catalysts

The textural properties of the prepared catalysts are presented in Table 1. The addition of promoters to Ni/Al_2O_3 catalyst increased the BET surface area. However, the K_2O-, CaO- and BaO-promoted catalysts exhibited almost the same BET surface areas. In addition, all the prepared catalysts showed high pore volume with small pore width in mesopore region [22].

Table 1. Structural properties of Ni/Al_2O_3 catalysts with different promoters

Catalysts	S_{BET}[a] ($m^2{\cdot}g^{-1}$)	Pore volume[b] ($cm^3{\cdot}g^{-1}$)	Pore width[c] (nm)
$7.5Ni/Al_2O_3$	252.4	0.56	6.6
$2K\text{-}7.5Ni/Al_2O_3$	309.6	0.55	5.9
$2Mg\text{-}7.5Ni/Al_2O_3$	271.9	0.59	6.4
$2Ca\text{-}7.5Ni/Al_2O_3$	305.0	0.69	6.7
$2Ba\text{-}7.5Ni/Al_2O_3$	312.0	0.65	6.7

[a]Calculated by the BET equation
[b]BJH desorption pore volume
[c]BJH desorption average pore diameter

The nitrogen adsorption/desorption isotherms and the pore size distributions are shown in Fig. 1(a) and 1(b), respectively. The sam-

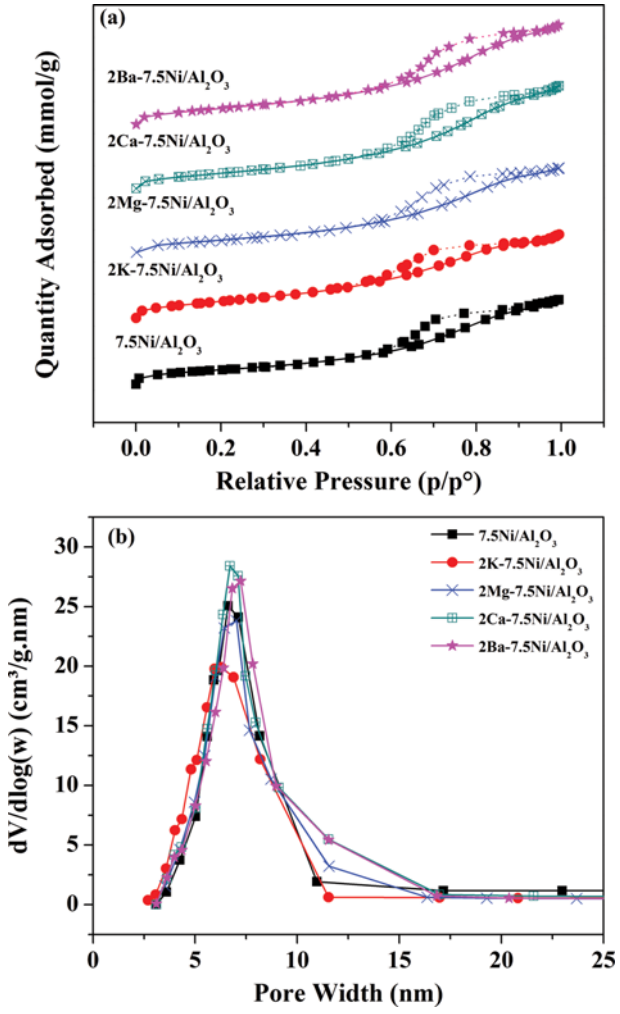

Fig. 1. (a) N_2 adsorption/desorption isotherms and (b) pore size distributions of the prepared catalysts.

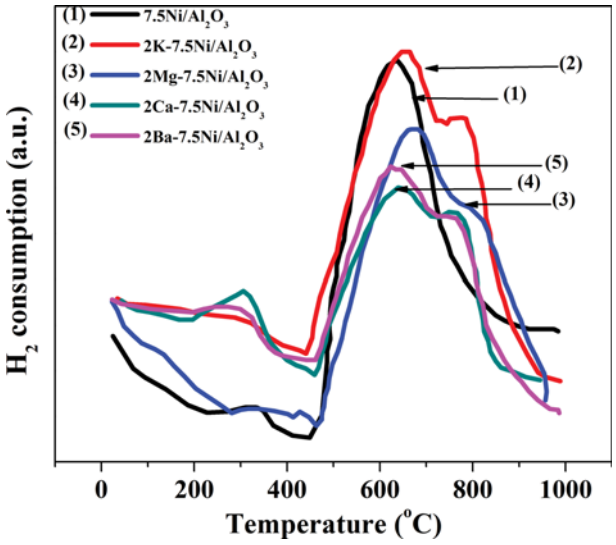

Fig. 2. H_2-TPR profiles of the prepared catalysts.

ples show IV type isotherm with H2 type hysteresis loop. According to IUPAC classification, this type of hysteresis loop is related to solids made of particles crossed by channels with cylindrical shape or consisting of spherical particles, which are aggregated (consolidated) or agglomerated (unconsolidated) with non-uniform size or shape [22]. The prepared samples showed pore size distribution in mesopore region in the range of 3-18 nm. The Ca- and Ba-promoted catalysts exhibited higher pore volume due to larger pore size distribution compared to other prepared catalysts.

The reduction behavior of the catalysts was investigated by TPR analysis (Fig. 2). In the TPR profile of the unpromoted catalyst, two reduction peaks were observed. The first reduction peak at 330 °C is related to reduction of bulk nickel oxide with a low interaction with alumina. The second reduction peak at around 630 °C is attributed to the reduction of nickel species with stronger interaction with alumina. Addition of promoters to nickel catalyst significantly affected the reduction behavior of nickel oxide. Depending on the type of promoter several reduction peaks with different intensities were observed. For the K_2O promoted catalyst the reduction peaks were observed at higher temperatures. The first peak at 640 °C is related to reduction of NiO with strong interaction with alumina and the second reduction peak at 800 °C belonged to reduction of $NiAl_2O_4$ spinel phase [23,24]. Addition of promoters decreased the intensity of the reduction peak related to bulk nickel oxide. In addition, the T_{max} of reduction peak for Ni/Al_2O_3 catalyst appeared at around 600 °C [22]; on the contrary the T_{max} of reduction peaks for the MgO, CaO and K_2O promoted catalysts was shifted to higher temperature and appeared at around 650 °C indicating the stronger interaction between NiO and Al_2O_3 in these promoted catalysts. Furthermore, addition of the promoters to nickel catalysts increased the amount of $NiAl_2O_4$ spinel phase. As mentioned, the peaks appearing at temperatures higher than 780 °C can be assigned to reduction of $NiAl_2O_4$ spinel phase. It seems that the amount of this spinel phase in K_2O promoted catalyst is higher compared to other promoted catalysts.

The catalytic behavior of the catalysts was investigated and the

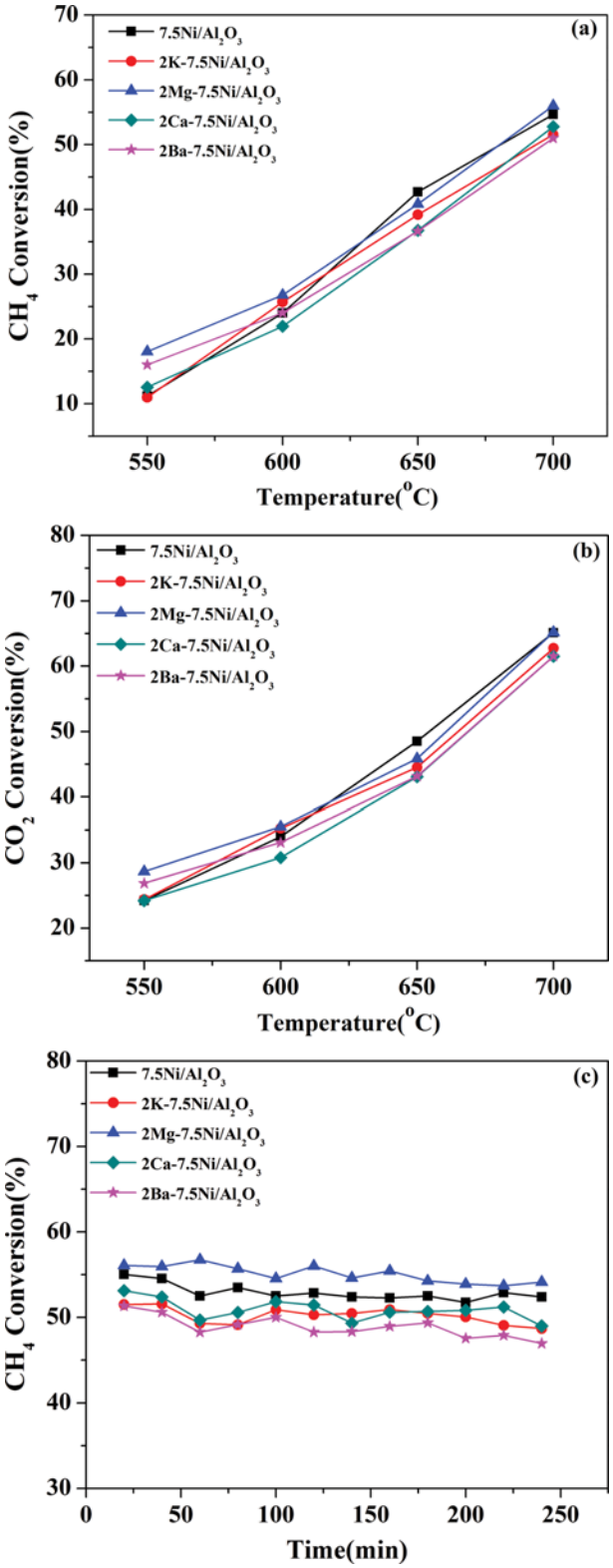

Fig. 3. (a) CH_4 conversion, (b) CO_2 conversion and (c) short time stability of the prepared catalysts. Reaction conditions: CH_4/CO_2=1 : 1, GHSV=18,000 (ml/h·g_{cat}).

results are illustrated in Fig. 3. The results showed that the MgO promoted catalyst exhibited higher conversion at 550, 600 and 700 °C.

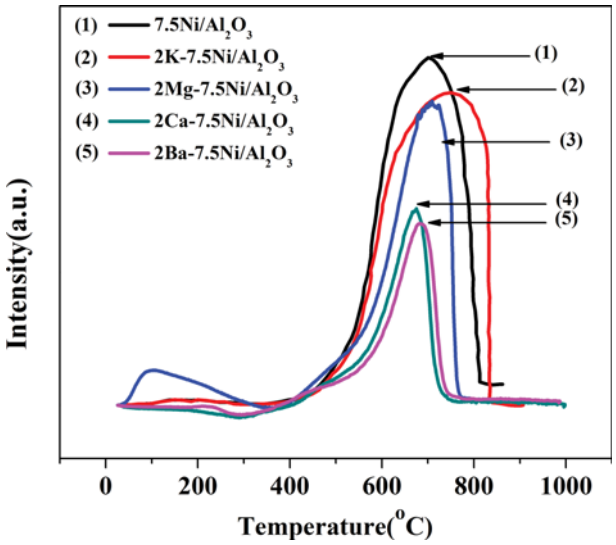

Fig. 4. TPO profiles of the spent catalysts. Reaction conditions: CH_4/CO_2=1, GHSV=18,000 (ml/h·g_{cat}).

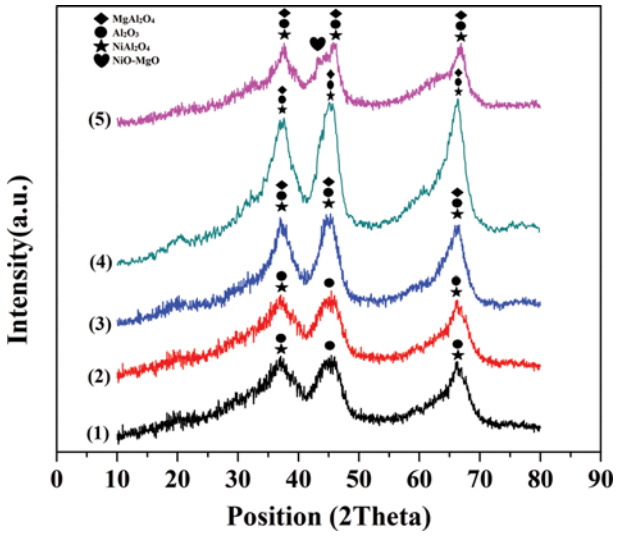

Fig. 5. XRD patterns of (1) 7.5Ni/Al_2O_3, (2) 2Mg-7.5Ni/Al_2O_3, (3) 4Mg-7.5Ni/Al_2O_3, (4) 6Mg-7.5Ni/Al_2O_3 (imp.), (5) 6Mg-7.5Ni/Al_2O_3 (struc.).

It seems that the CaO promoted catalyst showed higher conversion at 550 °C compared to unpromoted catalyst. The CO_2 conversions of the catalysts are also shown in Fig. 3(b). The results showed higher CO_2 conversion compared to CH_4 conversion due to the occurrence of the reverse water gas shift reaction ($CO_2+H_2 \leftrightarrow CO+H_2O$).

The short time stability of the catalysts is depicted in Fig. 3(c). As can be seen, all catalysts are almost stable. However, it seems that the MgO promoted catalyst exhibited higher stability compared to other catalysts.

TPO analysis was conducted to study the amount of deposited carbon over the spent catalysts, Fig. 4. Only one oxidation peak was observed for the spent catalysts. The observed peak in all catalysts occurred around 680 °C, attributed to filamentous form of carbon [22,25]. Oxidation of carbonaceous species started at around 400 °C. The results confirmed that the addition of promoters to nickel catalyst improved the resistance of catalysts against carbon formation. This can be related to the increasing in basicity of the catalyst due to the increasing of carbon dioxide adsorption on the catalyst surfaces [23]. This process can inhibit the CO decomposition and suppress the coke formation [26].

In this study, when the catalyst with the best performance was determined, the effect of different promoting routes was considered. For this purpose the MgO promoter was added to 7.5Ni/Al_2O_3 catalyst with two different methods. In the first method, the MgO was added to 7.5Ni/Al_2O_3 catalyst with impregnation method (6Mg-7.5Ni/Al_2O_3 (imp.)), and in the second method the MgO was added to microemulsion system during the preparation of 7.5Ni/Al_2O_3 catalyst (6Mg-7.5Ni/Al_2O_3 (struc.)).

XRD profiles of the prepared catalysts with various Mg contents are shown in Fig. 5. It is seen that the catalyst support has γ-Al_2O_3 crystalline structure. In all catalysts, diffraction peaks at 2θ= 38.06° and 66.2° are related to $NiAl_2O_4$ phase (code N. 01-1299) [22], and diffraction peaks at 2θ=37.4°, 46.07° and 66.9° are related to alumina phase (code N. 01-1303). It is known that the γ-Al_2O_3 has a pseudospinel crystalline structure and the lattice parameters of γ-Al_2O_3 are very close to that of $NiAl_2O_4$. In the 4Mg-7.5Ni/Al_2O_3 and 6Mg-7.5Ni/Al_2O_3 (imp.) catalysts, the formation of magnesium aluminate spinel ($MgAl_2O_4$) was observed (code N. 70-5187) and no other separate phases related to MgO were observed. The formation of MgO-NiO solid solution was observed in the 6Mg-

Table 2. Structural properties of the catalysts

Catalysts	S_{BET}[a] ($m^2 \cdot g^{-1}$)	Pore volume[b] ($cm^3 \cdot g^{-1}$)	Pore width[c] (nm)	Crystallite size[d] (nm)
7.5Ni/Al_2O_3	252.4	0.56	6.6	5.3
2Mg-7.5Ni/Al_2O_3	271.9	0.59	6.4	5.4
4Mg-7.5Ni/Al_2O_3	233.4	0.53	6.4	7.4
6Mg-7.5Ni/Al_2O_3 (imp.)	218.7	0.44	6.1	7.8
6Mg-7.5Ni/Al_2O_3 (struc.)	333.7	0.56	7.0	10.3

[a]Calculated by the BET equation
[b]BJH desorption pore volume
[c]BJH desorption average pore diameter
[d]Average crystalline diameter using Scherer equation from XRD

$7.5Ni/Al_2O_3$ (struc.) catalyst (code N. 24-0712). MgO and NiO both have face-centered-cubic structure and similar cation charges [27, 28]. In this system appearance of solid solution is very common. The diffusion of NiO to MgO lattice mostly took place. In the 6Mg-$7.5Ni/Al_2O_3$ catalysts the migration of Mg into the structure of alumina leads to formation of $MgAl_2O_4$.

The textural properties of the catalysts are presented in Table 2. The Debye-Scherrer equation (Eq. (1)) was employed for determining the average crystallite size of the samples.

$$D = \frac{0.9\lambda}{\beta\cos\theta} \quad (1)$$

In this equation, λ is the X-ray wavelength, θ is the Bragg angle and β is the pure full width of the diffraction line at half the maximum intensity.

The catalysts exhibited very high specific surface area and pore volume with small crystallite size. The results showed that with increasing in MgO content both the surface area and pore volume decreased. The decrease in specific surface area and pore volume is due to partial blockage or collapse of the pores of catalyst support by MgO clusters [29]. The surface area of 6Mg-$7.5Ni/Al_2O_3$ (struc.) is greater than the other ones. This may be related to the production process of this catalyst. The microemulsion in structural promoting procedure prepares an excellent environment and for this reason the microemulsion promoted catalyst showed high surface area [30]. With increasing the MgO content, the crystallite size of the samples also increased. The surface area of 6Mg-7.5 Ni/Al_2O_3 (struct.) was higher than that of 6Mg-7.5 Ni/Al_2O_3 (imp.). However, mesopore volume in 6Mg-7.5 Ni/Al_2O_3 (struct.) was smaller than that of 6Mg-7.5 Ni/Al_2O_3 (imp.). This phenomenon might be the result of more partial collapse or blockage of the pores of catalyst support during preparation process.

The N2 isotherms are plotted in Fig. 6(a). All isotherms exhibited a type IV with H2 shaped hysteresis loop. Furthermore, the pore size distributions of these samples are shown in Fig. 6(b). All samples exhibited mesoporous structure with pore size distribution centered around 7 nm. The available pore volume of the catalysts decreased and this occurrence can be related to increase of MgO content.

The reduction behavior of the catalysts was investigated by TPR analysis and the results are shown in Fig. 7. The unpromoted catalyst showed only one reduction peak in the temperature region of about 500-900 °C. This peak was attributed to reduction of nickel oxide with strong interaction with Al_2O_3. Another reduction peak at high temperature in TPR profile of the promoted catalysts is an indication of strong interaction between NiO and Al_2O_3, which may result from high dispersion of nickel particles over the catalyst support. The strong interaction of nickel with catalyst support can inhibit the Ni sintering. The close interaction between NiO and Al_2O_3 at a high temperature can cause the formation of nickel aluminate as shown in XRD analysis. It was suggested that the prepared catalysts with microemulsion method are a composite of NiO and $NiAl_2O_4$ [31]. The 2Mg-$7.5Ni/Al_2O_3$, 4Mg-$7.5Ni/Al_2O_3$, 6Mg-$7.5Ni/Al_2O_3$ (imp. and struc.) showed two major reduction peaks.

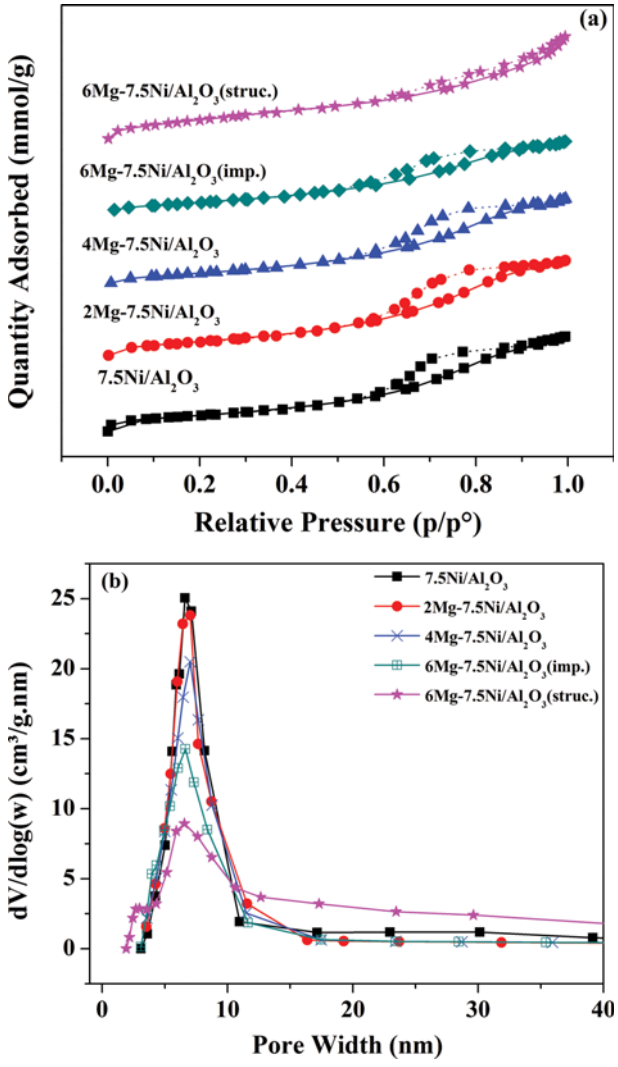

Fig. 6. (a) N_2 adsorption/desorption isotherms and (b) pore size distributions of the calcined catalysts.

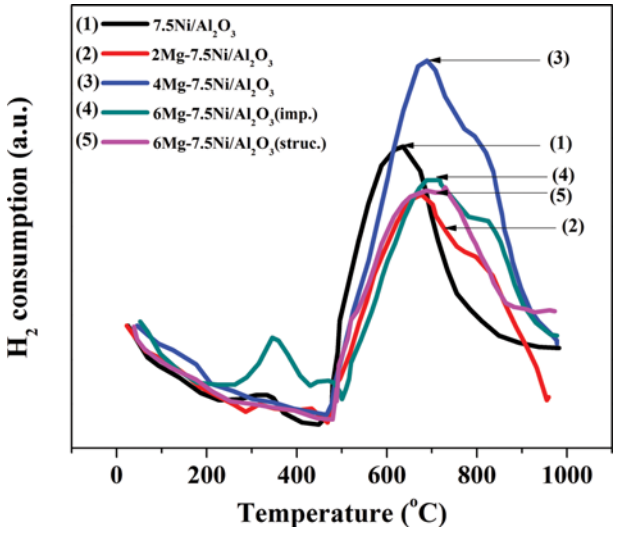

Fig. 7. TPR patterns of promoted catalysts with different promoter loadings.

The first one at about 680 °C is related to reduction of nickel oxide with high interaction with alumina. Second peak at temperature higher than 800 °C is related to reduction of $NiAl_2O_4$ [9,23,32,33]. The TPR profile demonstrates increasing in MgO content shifted the reduction temperature to higher temperatures.

The conversions of CH_4 and CO_2 are shown in Fig. 8(a) and 8(b), respectively. The obtained results show that the 6Mg-7.5Ni/Al_2O_3 (imp.) has the highest catalytic performance. CO_2 conversions were also higher than that of CH_4 due to occurrence of reverse water gas shift reaction. The catalytic stability test was conducted and demonstrated all catalysts had high stability with time on stream. The catalytic activity of the conventional 7.5 wt%Ni/Al_2O_3 catalyst prepared by impregnation method is shown in Fig. 8(a) and (b). The results show that this catalyst exhibited lower activity compared to the catalyst prepared by microemulsion method.

Fig. 9 shows the effect of gas hourly space velocity (GHSV) on the catalytic characteristics of 6Mg-7.5Ni/Al_2O_3 (imp.) catalyst at 700 °C (CH_4/CO_2=1). The results reveal that increasing in GHSV

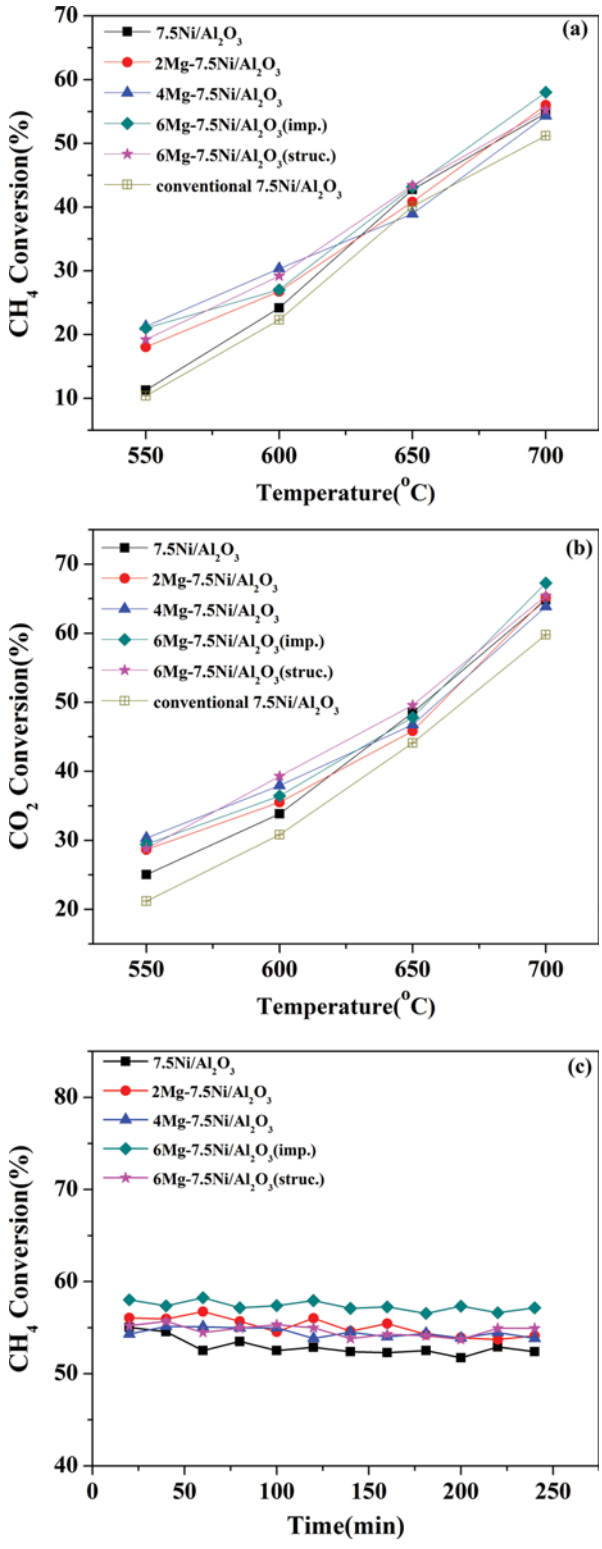

Fig. 8. (a) CH_4 conversion, (b) CO_2 conversion, (c) short time stability of the promoted catalysts with different promoter contents. Reaction conditions: CH_4/CO_2=1 : 1, GHSV=18,000 (ml/h·g_{cat}).

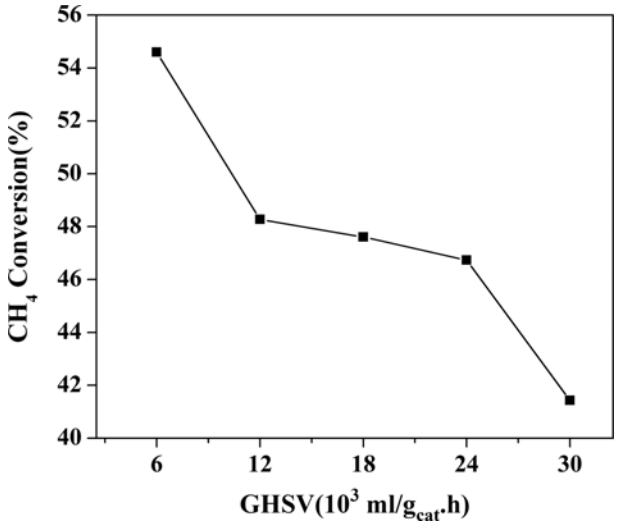

Fig. 9. Effect of GHSV on the catalytic activity of 6Mg-7.5Ni/Al_2O_3 (imp.) catalyst at 700 °C and CH_4/CO_2=1 : 1.

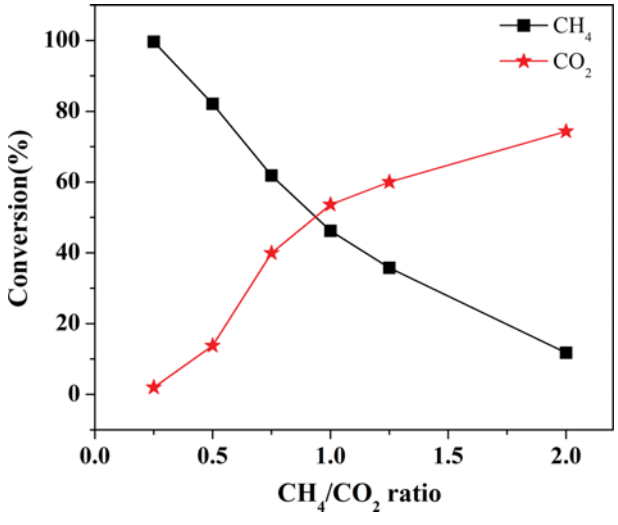

Fig. 10. Effect of feed ratio on the catalytic performance of 6Mg-7.5Ni/Al_2O_3 (imp.) at 700 °C and GHSV=18,000 (ml/h·g_{cat}).

has a negative effect on the catalytic performance due to the decrease in contact time and the amount of adsorbed reactants.

The influence of the feed ratio on the 6Mg-7.5Ni/Al_2O_3 (imp.) catalyst at 700 °C is shown in Fig. 10. The obtained results reveal that when the CH_4/CO_2 ratio increased from 1 : 4 to 2 : 1, the CH_4 conversion decreased. However, the CO_2 conversion increased due to less amount of CO_2 in the main reaction ($CH_4+CO_2 \leftrightarrow 2CO+2H_2$). Furthermore, as the CO_2/CH_4 ratio increased the molar ratio of H_2/CO decreased, due to higher extent of the RWGS reaction at higher CO_2/CH_4 ratios.

The TPO analysis of the spent catalysts is shown in Fig. 11(a). Only one peak was observed in the TPO profile of the spent catalysts. CO dissociation is the main reaction for carbon deposition [34]. In addition, the coke deposition was reduced in all promoted catalysts. With increasing the Lewis basicity of support and catalyst, the chemisorption of CO_2 increased and hence the equilibrium concentrations changed and carbon formation decreased [27,35]. The observed peak at around 680 °C is attributed to filamentous form of carbon [25]. The produced carbon is graphitic type [36]. Zhang et al. [37] employed several surface analysis techniques to study the type of carbon species formed on 17 wt% Ni/γ-Al_2O_3 and 17 wt% Ni/La_2O_3 catalysts. They found that the surface carbon on the spent Ni/γ-Al_2O_3 catalyst was dominated by graphitic -C-C- species, which can block the entire Ni surface, leading to the total loss of activity. From this analysis, the 6Mg-7.5Ni/Al_2O_3 (imp.) catalyst exhibited the lowest degree of carbon formation, due to higher basicity of this catalyst.

TPO analysis was employed for the spent 6Mg-7.5Ni/Al_2O_3 (imp.) catalyst after 10 h time on stream and the result is shown in Fig. 11(b). The obtained results reveal that one kind of carbon accumulated on the surface of catalyst after reaction. From the TPO analysis the observed peak at 700 °C may be related to filamentous type of carbon.

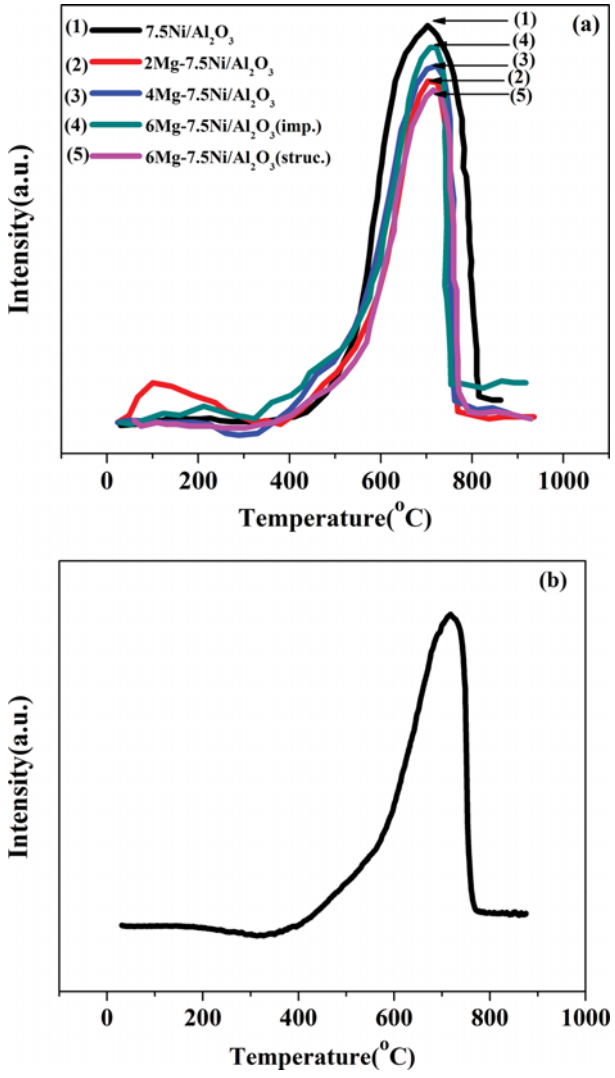

Fig. 11. TPO profiles of (a) the spent catalysts and (b) 6Mg-7.5Ni/Al_2O_3 (imp.) spent catalyst after 10 h time on stream at 700 °C. Reaction conditions: CH_4/CO_2=1, GHSV=18,000 (ml/h·g_{cat}).

CONCLUSION

The promoted 7.5 wt% Ni/Al_2O_3 catalysts were prepared by microemulsion method for dry reforming of methane. The addition of alkaline and alkaline earth promoters increased the surface areas of the catalysts. Among the prepared catalysts, the 2Mg-7.5Ni/Al_2O_3 catalyst showed the best catalytic performance. In addition, the 2Ba-7.5Ni/Al_2O_3 catalyst showed the best suppression of coke formation. The effect of different MgO loadings was investigated, and the results revealed with increasing in MgO content both the surface area and pore volume decreased. H_2-TPR analysis showed the formation of $NiAl_2O_4$ among the prepared catalyst. The 6Mg-7.5Ni/Al_2O_3 (imp.) showed the best catalytic activity and compared with 6Mg-7.5Ni/Al_2O_3 (struc.) catalyst in order to find the catalyst with the best performance. Results showed that although in-structural catalyst has a good activity, the 6Mg-7.5Ni/Al_2O_3 (imp.) has relatively higher methane conversion and stability. TPO profiles of spent samples exhibited the formation of filamentous form of carbon on the catalyst surface.

ACKNOWLEDGEMENTS

The authors gratefully acknowledge the support from Iran National Science Foundation (INSF) and University of Kashan for supporting this work by Grant No. 158426/98.

NOMENCLATURE

ME : microemulsion
XRD : X-ray diffraction
BET : Brunauer-Emmett-Teller surface area analysis
TPO : temperature programmed oxidation
SEM : scanning electron microscopy
TPR : temperature programmed reduction
BJH : Barrett-Joyner-Halenda pore size and volume analysis

REFERENCES

1. A. M. Gaddalla and M. E. Sommer, *Chem. Eng. Sci.*, **44**, 2825 (1989).

2. D. San-José-Alonso, J. Juan-Juan, M. Illán-Gómez and M. Román-Martínez, *Appl. Catal. A.*, **371**, 54 (2009).
3. B. Delmon, *Appl. Catal. B.*, **1**, 139 (1992).
4. W. Chen, G. Zhao, Q. Xue, L. Chen and Y. Lu, *Appl. Catal. B.*, **136**, 260 (2013).
5. Y. J. Asencios and E. M. Assaf, *Fuel Process. Technol.*, **106**, 247 (2013).
6. D. San José-Alonso, M. J. Illán-Gómez and M. d. C. Román-Martínez, *Int. J. Hydrogen Energy*, **38**, 2230 (2013).
7. V. Y. Bychkov, Y. P. Tyulenin, A. Firsova, E. Shafranovsky, A. Y. Gorenberg and V. Korchak, *Appl. Catal. A.*, **453**, 71 (2013).
8. H. Arandiyan, Y. Peng, C. Liu, H. Chang and J. Li, *J. Chem. Technol. Biotechnol.*, **89**, 372 (2014).
9. J. Zhu, X. Peng, L. Yao, J. Shen, D. Tong and C. Hu, *Int. J. Hydrogen Energy*, **36**, 7094 (2011).
10. H. Arandiyan, J. Li, L. Ma, S. Hashemnejad, M. Mirzaei, J. Chen, H. Chang, C. Liu, C. Wang and L. Chen, *J. Ind. Eng. Chem.*, **18**, 2103 (2012).
11. N. Majidian, N. Habibi and M. Rezaei, *Korean J. Chem. Eng.*, **31**, 1162 (2014).
12. J. Kim, T. Kim, J. W. Yoo, K. B. Lee and S. Hong, *Korean J. Chem. Eng.*, **29**, 1329 (2012).
13. M. Rezaei, S. M. Alavi, S. Sahebdelfar and Z.-F. Yan, *Energy Fuels*, **22**, 2195 (2008).
14. M. C. J. Bradford and M. A. Vannice, *Catal. Rev.*, **41**, 1 (1999).
15. C. Ping, H. Zhao-Yin and Z. Xiao-Ming, *Chin. J. Chem.*, **23**, 847 (2005).
16. H. S. A. de Sousa, A. N. da Silva, A. J. Castro, A. Campos, M. Josue Filho and A. C. Oliveira, *Int. J. Hydrogen Energy*, **37**, 12281 (2012).
17. W. Shen, H. Momoi, K. Komatsubara, T. Saito, A. Yoshida and S. Naito, *Catal. Today*, **171**, 150 (2011).
18. Y. H. Hu and E. Ruckenstein, *Adv. Catal.*, **48**, 297 (2004).
19. L. Coleman, W. Epling, R. Hudgins and E. Croiset, *Appl. Catal. A.*, **363**, 52 (2009).
20. M. Boutonnet, J. Kizling, P. Stenius and G. Maire, *Colloids Surf.*, **5**, 209 (1982).
21. M. A. Goula, N. D. Charisiou, K. N. Papageridis, A. Delimitis, E. Pachatouridou and E. F. Iliopoulou, *Int. J. Hydrogen Energy*, **40**, 9183 (2015).
22. M. H. Aboonasr Shiraz, M. Rezaei and F. Meshkani, *Can. J. Chem. Eng.*, **94**, 1177 (2016).
23. H.-S. Roh and K.-W. Jun, *Catal. Surv. Asia*, **12**, 239 (2008).
24. G. Zhong, *Angew. Chem. Int. Ed.*, **42**, 4247 (2003).
25. S. Wang and G. Q. M. Lu, *J. Chem. Technol. Biotechnol.*, **75**, 589 (2000).
26. M. García-Diéguez, C. Herrera, M. Á. Larrubia and L. J. Alemany, *Catal. Today*, **197**, 50 (2012).
27. O. Yamazaki, T. Nozaki, K. Omata and K. Fujimoto, *Chem. Lett.*, 1953 (1992).
28. Y.-H. Wang, H.-M. Liu and B.-Q. Xu, *J. Mol. Catal. A: Chem.*, **299**, 44 (2009).
29. A. Zhao, W. Ying, H. Zhang, H. Ma and D. Fang, *Catal. Commun.*, **17**, 34 (2012).
30. S. Eriksson, U. Nylén, S. Rojas and M. Boutonnet, *Appl. Catal. A.*, **265**, 207 (2004).
31. S. Xu, R. Zhao and X. Wang, *Fuel Process. Technol.*, **86**, 123 (2004).
32. K. Sutthiumporn and S. Kawi, *Int. J. Hydrogen Energy*, **36**, 14435 (2011).
33. K.-M. Kang, H.-W. Kim, I.-W. Shim and H.-Y. Kwak, *Fuel Process. Technol.*, **92**, 1236 (2011).
34. M. Bradford and M. Vannice, *Catal. Rev.*, **41**, 1 (1999).
35. G. J. Kim, D.-S. Cho, K.-H. Kim and J.-H. Kim, *Catal. Lett.*, **28**, 41 (1994).
36. S. Wang and G. Lu, *Ind. Eng. Chem. Res.*, **38**, 2615 (1999).
37. Z. Zhang, X. E. Verykios, S. M. MacDonald and S. Affrossman, *J. Phys. Chem.*, **100**, 744 (1996).